

## An Interval-Based Algorithm for Uncertainty Quantification in Composite Structures

Herbert M. Gomes\*, Pedro B. Santana\*, Ewerton Grotti\*.

\*(Department of Mechanical Engineering, UFRGS University, Av. Sarmiento Leite, 425, 2o. andar, Porto Alegre, RS, Brazil.

Corresponding author: Herbert M. Gomes

### ABSTRACT

Composite materials have been used extensively in the aeronautical and automotive industries. Despite the improved knowledge about the mechanical and dynamic behavior and modes of failure, it is still not well explained some variability from experimental data obtained for, a priori, and nominally identical specimens. Epistemic and aleatory uncertainties are alleged as the main causes for these discrepancies besides the uncertainties from modeling. Regarding the structural damping of such structures, the phenomena involved are not completely revealed nor modeled. This paper presents an interval-based algorithm for uncertainty quantification in composite structures. The  $\alpha$ -cut procedures are used to account for the several levels of uncertainty present in material properties, geometrical imperfections and external loading. Due to the lack of reliable statistical information about such uncertainties, the interval-based approach is used in this study and compared with the robust solution by Monte Carlo simulations.

**Keywords**-laminated composites, uncertainty, interval-based uncertainty, convex hull, buckling loads

DATE OF SUBMISSION: 15-01-2020

DATE OF ACCEPTANCE: 31-01-2020

### I. INTRODUCTION

Uncertainty in composite materials properties is a key problem when dealing with the manufacturing processes used to build stacks of layers that compose the final structure. Sensitivity to temperature, hygroscopic phenomena, and the own manufacturing process can deviate the overall behavior of the composite from the expected ones. Even the procedures and standardized tests used to characterize such elastic properties present some degree of uncertainty as explained by He et al. (2018). An extensive bibliography exists in quantifying these uncertainties like those discussed in Dey et al. (2018). In this paper, the developed algorithm is based on the  $\alpha$ -cut concept and convex hull from the quick hull algorithm (Barber et al., 1996) as explained in Faes et al. (2017).

In a simplified way, the robustness of interval analysis relies on the no assumption for probability distribution types, partially justified in the scarcity of data. Uncertainties on the limit values can be estimated based on this scarce data, but no detailed statistics of such distribution nor correlation between variables. For some uncertain parameters of the system, this propagates originating uncertainties in the measured and unmeasured output parameters that represent the behavior of the system. On the framework of Interval Approach, the measure of confidence on the uncertainty level of such variables can be associated to an  $\alpha$ -cut level (Figure 1(b)), a

single value that varies from 0 (maximum uncertainty in the interval limits) to 1 (complete confidence and thus, no uncertainty at all). Several simplified methods can be used to evaluate the propagation of such interval values (gradient-based methods, interval arithmetic, etc.) but none with sufficient accuracy for any level of uncertainty. This is particularly not true in the case of an anti-optimization approach. Based on the uncertain limits of the variables, one tries to maximize and minimize output variables that represent the behavior of the system and doing this is more prone to correctly define and evaluate such uncertain intervals. A simple Monte Carlo approach would also be useful in this concern, simulating, let's say, uniform random variables into the uncertain limits, but when comes to talk about performance and efficiency, this will not be the best choice as it will be explored later in the examples in this paper.

### II. UNCERTAINTY PROPAGATION AND ANTI-OPTIMIZATION

Let's assume a system with the input vector  ${}^m\mathbf{X} = ({}^m x_1, {}^m x_2, \dots, {}^m x_{n_i})^T$ , where  $n_i$  is the number of input variables,  $m$  means "measured" and an output vector as  ${}^m\mathbf{Z} = ({}^m z_1, {}^m z_2, \dots, {}^m z_{n_o})^T$ , where  $n_o$  is the number of output variables. Let's assume a number of samples of each one of the input vectors (called realizations)  ${}^m_1\mathbf{X}, {}^m_2\mathbf{X}, \dots, {}^m_s\mathbf{X}$  and the corresponding output vectors  ${}^m_1\mathbf{Z}, {}^m_2\mathbf{Z}, \dots, {}^m_s\mathbf{Z}$ , where

ns means the number of samples. Furthermore, let's assume a numerical model of the system with the same measured inputs  ${}^m\mathbf{X} = ({}^m x_1, {}^m x_2, \dots, {}^m x_{ni})^T$ , adjustable model's parameters vector  $\boldsymbol{\theta} = (\theta_1, \theta_2, \dots, \theta_{np})^T$ , with np representing the number of parameters and predicted vector outputs  ${}^p\mathbf{Z} = ({}^p z_1, {}^p z_2, \dots, {}^p z_{no})^T = f({}^m\mathbf{X}, \boldsymbol{\theta})$ . Related to the output vector, it is easy to obtain their upper and lower bounds based on the values from all realizations. These output intervals vector may be put together in a two-column vector representation as:

$$[{}^m\mathbf{z}, {}^m\bar{\mathbf{z}}] = [ \min_{i=1, \dots, ns} ({}^m_i\mathbf{z}) \quad \max_{i=1, \dots, ns} ({}^m_i\mathbf{z}) ] \quad (1)$$

this represents a measure of the model's output uncertainty or dispersion. The same can be stated for the predicted output vector (from the numerical model) and the measured input vector:

$$[{}^m\mathbf{X}, {}^m\bar{\mathbf{X}}] = [ \min_{i=1, \dots, ns} ({}^m_i\mathbf{X}) \quad \max_{i=1, \dots, ns} ({}^m_i\mathbf{X}) ] \quad (2)$$

$$[\boldsymbol{\theta}, \bar{\boldsymbol{\theta}}] = [ \min_{i=1, \dots, ns} ({}_i\boldsymbol{\theta}) \quad \max_{i=1, \dots, ns} ({}_i\boldsymbol{\theta}) ] \quad (3)$$

$$[{}^p\mathbf{z}, {}^p\bar{\mathbf{z}}] = f([{}^m\mathbf{X}, {}^m\bar{\mathbf{X}}], [\boldsymbol{\theta}, \bar{\boldsymbol{\theta}}]) = [ \min_{i=1, \dots, ns} ({}^p_i\mathbf{z}([\boldsymbol{\theta}, \bar{\boldsymbol{\theta}}])) \quad \max_{i=1, \dots, ns} ({}^p_i\mathbf{z}([\boldsymbol{\theta}, \bar{\boldsymbol{\theta}}])) ] \quad (4)$$

At each hyper quadrant

Find  $\mathbf{X}^*, \boldsymbol{\theta}^*$  that minimizes and maximizes  $\|\mathbf{Z}^*\|_2$ .

Subject to :  $\mathbf{X}^* \in [{}^m\mathbf{X}, {}^m\bar{\mathbf{X}}], \boldsymbol{\theta}^* \in [\boldsymbol{\theta}, \bar{\boldsymbol{\theta}}]$  and  $[\mathbf{z}, \bar{\mathbf{z}}] = [ \min_{\text{in all quadrants}} (\mathbf{z}^*) \quad \max_{\text{in all quadrants}} (\mathbf{z}^*) ] \quad (5)$

In this case, where a double optimization happens, the number of design variables is (ni+np). A block diagram can be sketched in this sense, as represented in Figure 1(a).

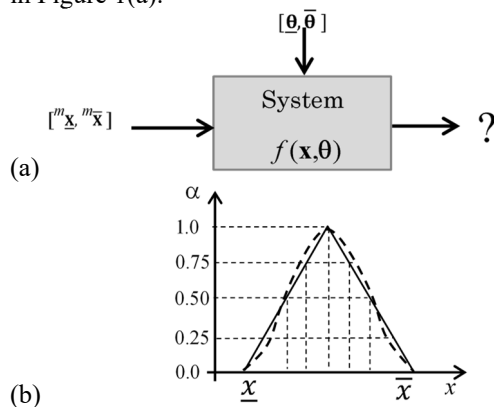


**Figure 1** – (a) Interval uncertainty propagation. (b) Linear approximation of Gaussian distribution for x by a triangular fuzzy-set, with uncertain intervals and  $\alpha$ -cuts.

The interval upper and lower values form a cloud in the hyperspace and, once obtained, a convenient way to visualize in constructing a convex hull, which is the smallest convex set that contains

and encompasses the set of points. This convex hull can also be constructed, if Monte Carlo Methods are used, for the random points obtained by the simulations.

### III. COMPOSITE MATERIAL

The differential equations for a laminated plate can be derived from analyzing Figure 2, where a force diagram is depicted (comma represents the corresponding partial derivatives). By the resulting forces in x and y directions, we find (i)  $N_{x,x} + N_{xy,x} = 0$  and (ii)  $N_{y,y} + N_{xy,y} = 0$ . Considering the inertia force (density  $\rho$  and height  $h$ ) and the forces in the z-direction, one finds the equilibrium equation  $Q_{x,x} + Q_{y,y} + N_x w_{,xx} + 2N_{xy} w_{,xy} + N_y w_{,yy} - \rho h w_{,tt} = 0$ . For the moment equations and neglecting the third-order terms, one finds  $M_{x,x} + M_{xy,y} = Q_x$  and  $M_{y,y} + M_{xy,x} = Q_y$  that results in (iii)  $M_{x,xx} + 2M_{xy,xy} + M_{y,yy} + N_x w_{,xx} + 2N_{xy} w_{,xy} + N_y w_{,yy} - \rho h w_{,tt} = 0$ .

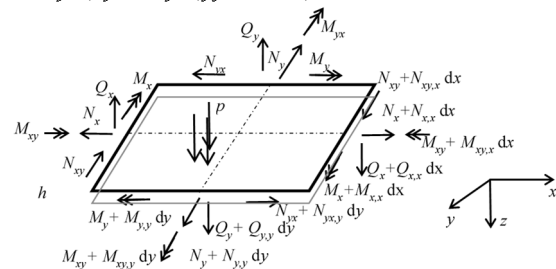


**Figure 2** – Force diagram at the middle surface of a laminated plate.

This forms a set of three differential equations of motion. For a laminated plate, the constitutive relations for stress/strains at the local coordinate system for laminate k at height z is (assuming First-Order Shear Deformation Theory, FSDT):

$$\begin{Bmatrix} \sigma_x \\ \sigma_y \\ \tau_{xy} \end{Bmatrix}_k = \begin{bmatrix} \bar{Q}_{11} & \bar{Q}_{12} & \bar{Q}_{16} \\ \bar{Q}_{12} & \bar{Q}_{22} & \bar{Q}_{26} \\ \bar{Q}_{16} & \bar{Q}_{26} & \bar{Q}_{66} \end{bmatrix}_k \left( \begin{Bmatrix} \epsilon_x^0 \\ \epsilon_y^0 \\ \gamma_{xy}^0 \end{Bmatrix} + z \begin{Bmatrix} k_x \\ k_y \\ k_{xy} \end{Bmatrix} \right) \quad (6)$$

and the internal forces evaluated as:

$$\begin{Bmatrix} N_x \\ N_y \\ N_{xy} \end{Bmatrix} = \int_{-t/2}^{+t/2} \begin{Bmatrix} \sigma_x \\ \sigma_y \\ \tau_{xy} \end{Bmatrix}_k dz, \quad \begin{Bmatrix} M_x \\ M_y \\ M_{xy} \end{Bmatrix} = \int_{-t/2}^{+t/2} z \begin{Bmatrix} \sigma_x \\ \sigma_y \\ \tau_{xy} \end{Bmatrix}_k dz \quad (7)$$

and applying Equation (6), one recovers:

$$\begin{Bmatrix} N_x \\ N_y \\ N_{xy} \end{Bmatrix} = \mathbf{A}_{ij} \begin{Bmatrix} \epsilon_x^0 \\ \epsilon_y^0 \\ \gamma_{xy}^0 \end{Bmatrix} + \mathbf{B}_{ij} \begin{Bmatrix} k_x \\ k_y \\ k_{xy} \end{Bmatrix}, \quad \begin{Bmatrix} M_x \\ M_y \\ M_{xy} \end{Bmatrix} = \mathbf{B}_{ij} \begin{Bmatrix} \epsilon_x^0 \\ \epsilon_y^0 \\ \gamma_{xy}^0 \end{Bmatrix} + \mathbf{D}_{ij} \begin{Bmatrix} k_x \\ k_y \\ k_{xy} \end{Bmatrix} \quad (8)$$

The matrices **A**, **B** and **D** are evaluated as usual, along each ply, as  $A_{ij} = \sum_{k=1}^n \kappa (\bar{Q}_{ij})_k (z_k - z_{k-1})$ ,  $B_{ij} = \frac{1}{2} \sum_{k=1}^n (\bar{Q}_{ij})_k (z_k^2 - z_{k-1}^2)$  and  $D_{ij} = \frac{1}{3} \sum_{k=1}^n (\bar{Q}_{ij})_k (z_k^3 - z_{k-1}^3)$  and  $\kappa = 5/6$ . Based on the Classical Laminated Theory, taking the strain displacement relationship, one finds:

$$\begin{Bmatrix} \epsilon_x^0 \\ \epsilon_y^0 \\ \gamma_{xy}^0 \end{Bmatrix} = +\mathbf{B}_{ij} \begin{Bmatrix} u_x \\ v_y \\ u_y + v_x \end{Bmatrix}, \quad \begin{Bmatrix} k_x \\ k_y \\ k_{xy} \end{Bmatrix} = \begin{Bmatrix} -w_{,xx} \\ -w_{,yy} \\ -2w_{,xy} \end{Bmatrix} \quad (9)$$

and finally, the set of the three differential equations, taking into consideration Equation (8) results in:

$$\begin{aligned} A_{11}u_{,xx} + 2A_{16}u_{,xy} + A_{66}u_{,yy} + A_{16}v_{,xx} \\ + (A_{11} + A_{66})v_{,xy} + A_{26}v_{,yy} \\ - B_{11}w_{,xxx} - 3B_{16}w_{,xxy} \\ - (B_{12} + 2B_{66})w_{,xyy} - B_{26}w_{,yyy} \\ = 0 \\ A_{16}u_{,xx} + (A_{12} + A_{66})u_{,xy} + A_{26}u_{,yy} + A_{66}v_{,xx} + \\ 2A_{26}v_{,xy} + A_{22}v_{,yy} - B_{22}w_{,yyy} = 0 \quad (10) \\ D_{11}w_{,xxxx} + 4D_{16}w_{,xxxxy} + 2(D_{12} + 2D_{66})w_{,xxyy} \\ + 4D_{26}w_{,xyyy} + D_{22}w_{,yyyy} \\ - B_{11}u_{,xxx} - 3B_{16}u_{,xxy} \\ - (B_{12} + 2B_{66})u_{,xyy} - B_{26}u_{,yyy} \\ - B_{16}v_{,xxx} - (B_{12} + 2B_{66})v_{,xxy} \\ - 3B_{26}v_{,xyy} - B_{22}v_{,yyy} + N_x w_{,xy} \\ + N_y w_{,yy} + \rho h w_{,tt} = 0 \end{aligned}$$

In the case of symmetrically angle-ply oriented composite plates,  $A_{16} = A_{26} = D_{16} = D_{26} = B_{ij} = 0$  and the previous equations simplify. To solve such equation one can use the separability of space and time with Fourier series in the form:  $w(x, y, t) = [\alpha_{mn} \cos(\omega t) + \beta_{mn} \sin(\omega t)] X_m(x) Y_n(y)$  and considering the corresponding boundary conditions, results in a system of equations that will give the natural frequencies and mode shapes, only if a nontrivial solution exists. In this case, for a simply supported plate with edges  $a$  and  $b$ , the following equation for natural frequencies results:

$$\omega_{m,n}^2 = \frac{\pi^4}{\rho h} \left[ D_{11} \left(\frac{m}{a}\right)^4 + 2(D_{12} + 2D_{66}) \left(\frac{m}{a}\right)^2 \left(\frac{n}{b}\right)^2 + D_{22} \left(\frac{n}{b}\right)^4 \right] \quad (11)$$

where  $m$  and  $n$  are positive integers that should be tried to get each of the mode frequencies.

Assuming that the only applied load are those from in-plane and taking the effects in the total potential energy split into two parts, bending and external forces ( $\Pi = U_b + U_p$ ), one can evaluate those parts for an assumed field solution that accounts for boundary conditions of the form of sine series. In the case of a simply supported plate, it assumes the form  $w(x, y) = w_{mn} \sin(m\pi x/a) \sin(n\pi y/b)$  with  $w_{mn}$  being the displacement coefficients and  $m, n$ , positive integers. Substituting this assumed displacement field into the total

potential energy, forcing a stationary condition ( $\partial \Pi / \partial w_{mn} = 0$ ) and solving for  $\lambda = N_{crit} / N_x$  (critical to the reference applied load ratio), the buckling loads are computed. In fact, the first buckling load is of interest, and one should search for the combinations of  $m$  and  $n$  that gives the lower  $\lambda$  (first buckling load). In case of a simply supported plate with two in-plane loads  $N_x$  and  $N_y$ , the resulting expression is:

$$\lambda_{m,n} = \frac{C_1 C_5^2 + \alpha C_3 C_2^2 + \beta C_5 C_2^2 + C_4 C_3^2 - \alpha C_1 C_3 C_4 - \beta C_1 C_4 C_5 - 2 C_2 C_3 C_5}{\alpha^2 (C_1 C_4 - C_2^2) + \zeta \beta^2 (C_1 C_4 - C_2^2)} \quad (12)$$

where  $\zeta = N_y / N_x$  and  $C_1 = -D_{11} \alpha^2 - D_{66} \beta^2 - A_{55} k$ ,  $C_2 = -D_{12} \alpha \beta - D_{66} \alpha \beta$ ,  $C_3 = -A_{55} k \alpha$ ,  $C_4 = -D_{22} \beta^2 - D_{66} \alpha^2 - A_{44} k$  and  $C_5 = -A_{44} k \beta$ ,  $\alpha = m\pi/a$ ,  $\beta = n\pi/b$ .

#### IV. COMPOSITE MATERIAL UNCERTAINTIES

There are some unavoidable uncertainties in composite manufacturing, such as intra-laminate voids, incomplete curing of the resin and excess resin between plies, porosity, excess matrix voids, variations in ply thickness and fiber parameters, all those making the overall behavior and prediction of such materials difficult. In this study, only mass density, ply angle orientation and Elastic modulus values will be considered with uncertain values since those are the most important source of the variability described in the literature (Dey et al., 2018).

##### 4.1 Numerical Examples

The following example shows a composite with the total length and breadth of the laminated plate with orthotropic cross-ply  $[90^\circ/0^\circ/0^\circ/90^\circ]$  configuration, and dimensions  $a=0.6$  m and  $b=0.6$  m and laminate thickness of  $t=0.125$  mm. The material properties of the laminate are  $E_{11}=1.35 \times 10^{11}$  Pa,  $E_{22}=8.8 \times 10^9$  Pa,  $G_{12}=4.8 \times 10^9$  Pa,  $\nu_{12}=0.33$  and  $\rho=1380$  kg/m<sup>3</sup>. The boundary conditions are simply supported on each side (SSSS).

In this examples it is assumed an interval uncertainty of  $\pm 10\%$ , for the worst-case scenario (corresponding to  $\alpha$ -cut level 0) in  $E_{11}$ ,  $\rho$ ,  $G_{12}$  and an uncertainty  $\pm 5^\circ$  for  $\theta$ . This uncertainty is assumed independent for each layer, so the number of uncertainties are 16 in total. The proposed algorithm is tested using the interval approach proposed in this paper and compared with simple MC (Monte Carlo simulations). For fair comparisons, the number of MC simulations equals the number of function calls used in the Interval-based proposed algorithm (that runs first). The uncertainty in the dynamic behavior is sought in this example so, the first four natural frequencies are evaluated. The analytical solutions for the deterministic situation for this particular case are given by Equation (10). The following Figure 1 is

obtained for the convex-hulls for the first 4 natural frequencies ( $y_1=f_1$ ,  $y_2=f_2$ ,  $y_3=f_3$  and  $y_4=f_4$  in Hz).

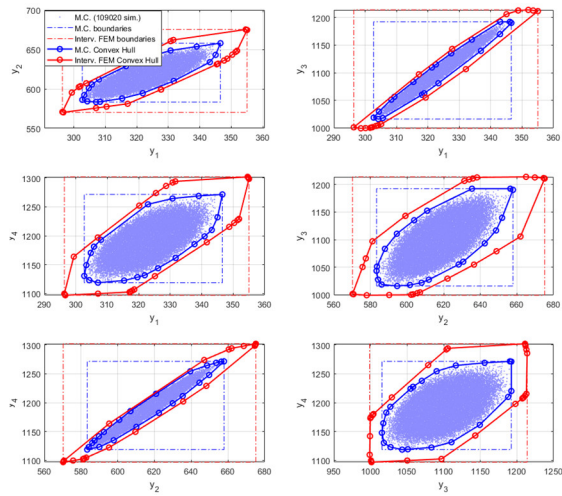


**Figure 3** – Output uncertain intervals and convex hulls for the interval-based procedure and MC Simulation for mode frequencies.

Table 1 shows the relative differences between the Interval-based Method interval method proposed here and the traditional Monte Carlo Method based on the Error (E) values defined as the ratio between twice the Interval Radius of the uncertain output variables (first 4 mode frequencies) for the zero  $\alpha$ -cut level and the Interval Center. The Interval Radius for an uncertain variable  $z$  is defined as  $IR = (\bar{z} - \underline{z})/2$ , while the Interval Center is defined as  $IC = (\bar{z} + \underline{z})/2$ , so  $E = 2 IR/IC$ .

**Table 1** – Error-values for interval output variables obtained by the Interval-based Method and the MC method.

Mode Frequency (Hz)	Interval-based Method			MC Method		
	Lower bound $\underline{f}$	Upper bound $\bar{f}$	E (%)	Lower bound $\underline{f}$	Upper bound $\bar{f}$	E (%)
$f_1$	$2.9635 \times 10^2$	$3.5503 \times 10^2$	18.22	$3.0268 \times 10^2$	$3.4657 \times 10^2$	13.63
$f_2$	$5.7025 \times 10^2$	$6.7518 \times 10^2$	17.07	$5.8334 \times 10^2$	$6.5786 \times 10^2$	12.12
$f_3$	$9.9929 \times 10^2$	$1.2130 \times 10^3$	19.41	$1.0157 \times 10^3$	$1.1924 \times 10^3$	16.05
$f_4$	$1.0970 \times 10^3$	$1.3021 \times 10^3$	17.26	$1.1188 \times 10^3$	$1.2716 \times 10^3$	12.87

Analyzing Table 1, one can notice the spread of the results obtained with Interval-based Method when compared to the MC method since E values are greater (5% on average). This also can be noticed by the graphs of Figure 3, where the convex hull and interval limits for the Interval-based Method encompass the corresponding values for the MC Method. The numerical evaluations took less than 100 seconds in a computer i9-3.6 GHz with 32 GB RAM.

The second example is intended to investigate the uncertainty in the first four buckling loads in the cross-ply  $[90^\circ/45^\circ/0^\circ/45^\circ/90^\circ]$  of a simply supported plate. In this case, the mass density is not assumed uncertain since it does not collaborate with the buckling load. It is assumed the same

uncertainty of  $\pm 5^\circ$  for  $\theta$  at each layer and uncertainty of  $\pm 10\%$ , (for  $\alpha$ -cut level 0) in  $E_{11}$ ,  $G_1$  and  $\nu_{12}$ . For the buckling analysis, it is assumed  $N_y=N_x$  (equal compressive load). Figure 4 is obtained for the convex-hulls for the first 4 buckling loads, where  $y_1=\lambda_1$ ,  $y_2=\lambda_2$ ,  $y_3=\lambda_3$  and  $y_4=\lambda_4$  that are dimensionless. For comparisons purposes, Table 2 shows the differences in for the interval FEM and the Monte Carlo results in terms of the Error values.

**Table 2** – Error-values for interval output variables obtained by the Interval-based Method and the MC method.

Buckling load ratio	Interval-based Method			MC Method		
	Lower bound $\underline{\lambda}$	Upper bound $\bar{\lambda}$	E (%)	Lower bound $\underline{\lambda}$	Upper bound $\bar{\lambda}$	E (%)
$\lambda_1$	$5.7114 \times 10^6$	$7.0246 \times 10^6$	20.73	$5.8045 \times 10^6$	$6.8921 \times 10^6$	17.17
$\lambda_2$	$7.2834 \times 10^6$	$9.7252 \times 10^6$	29.20	$7.5910 \times 10^6$	$9.4138 \times 10^6$	21.80
$\lambda_3$	$1.1425 \times 10^7$	$1.5950 \times 10^7$	33.81	$1.1895 \times 10^7$	$1.5448 \times 10^7$	26.55
$\lambda_4$	$1.7598 \times 10^7$	$2.5082 \times 10^7$	35.93	$1.8282 \times 10^7$	$2.4329 \times 10^7$	29.04

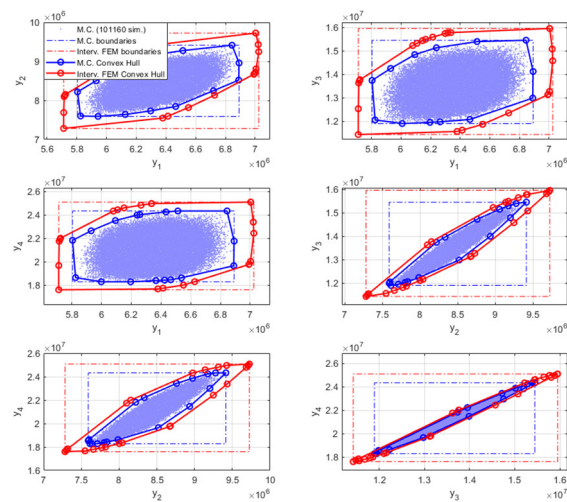


**Figure 4** – Output uncertain intervals and convex hulls for the Interval-based procedure and MC Simulation for buckling loads (dimensionless buckling ratio,  $\lambda = N_{crit}/N_x$ ).

Again, analyzing Table 2, one can notice the spread of the results obtained with Interval-based Method when compared to the MC method since E values are greater (3% on average).

## V. CONCLUSION

It was observed that the convex hulls as the output intervals are not well-defined when using traditional Monte Carlo Simulation. This is attributed to the fact that the worst scenario is a precise combination of values of uncertain input variables that cannot be obtained by simple random simulations. Despite the huge amount of simulations, the extreme (worst-case scenario) is correctly defined only by the Interval based methodology proposed in this paper. In the examples analyzed, mode frequencies and buckling loads, the Interval based methodology presented 5% to 3% larger Error values when compared to the Monte Carlo Method,

which means a larger uncertain area.

### ACKNOWLEDGEMENTS

The authors thank CNPq and CAPES for the partial financial support for this research.

### REFERENCES

- [1]. T. Hea, L. Liua, A. Makeev. Uncertainty analysis in composite material properties characterization using DIC and finite element model updating. *Comp. Struct.*, 184, (2018), 337-351.
- [2]. S. Dey, T.Mukhopadhyay, S.Adhikari. Uncertainty quantification in laminated composites: a meta-model based approach. CRC Press.
- [3]. M.Faes, D.Moens. Identification and quantification of spatial interval uncertainty in numerical models. *Comp. Struct.*, 192, (2017), 16-33.
- [4]. C.B. Barber, D.P. Dobkin, H.Huhdanpaa. The quick hull algorithm for convex hulls. *ACM Trans Math Soft.* 22(4). 1996, 469–83.
- [5]. Y.Luo, M.Hong, Y.Liu. Analytical solutions to the Fundamental frequency of arbitrary laminated plates under various boundary conditions. *J. of Marine Sc. Appl.* 2015, 14: 46-52.

Herbert M. Gomes, et.al. “An Interval-Based Algorithm for Uncertainty Quantification in Composite Structures” *International Journal of Engineering Research and Applications (IJERA)*, vol.10 (01), 2020, pp 46-50.